JOURNAL OF GEOPHYSICAL RESEARCH, VOL. 103, NO. B9, PAGES 21,183–21,200, SEPTEMBER 10, 1998

Mantle stratigraphy and evolution of the Slave province

M. G. Bostock

Department of Earth and Ocean Sciences, University of British Columbia, Vancouver, Canada

Abstract. A data set of 1033 three-component, P wave seismograms from five broadband stations at the Yellowknife Array is assembled to investigate mantle structure below the southern Slave province in Canada's Northwest Territories. Following wave field decomposition, seismograms are source-normalized through simultaneous deconvolution to estimate the near-receiver impulse response as a function of epicentral distance and back azimuth. Images of impulse response reveal a well-developed mantle stratigraphy, anisotropic in part, extending from the Mohorovicic discontinuity to the transition zone. A layer of depth-localized anisotropy ($\pm 5\%$), termed H, is situated between $\sim$ 70 and 80 km depth with an average shear velocity comparable to that of the ambient mantle and a sharp upper boundary less than 100 m in transition width. The absence of free surface crustal reverberations on the transverse component affords a window into the upper mantle between 100 and 200 km depth. A sequence of at least two layers between 120-150 km depth, collectively termed X, is most clearly evident to the north and is underlain by a second structure L which dips from 170 km in the west to 230 km into the center of the Slave province. The deepest interface above the transition zone W marks a shear velocity inversion near 350 km depth whose signature is restricted to the SV component signalling a dominantly isotropic response. Consideration of these observations in light of data acquired in a recent LITHOPROBE seismic reflection traverse and in petrological studies of kimberlite xenoliths prompts speculation into the role of subduction in craton stabilization. It is suggested that the proto-Slave craton was assembled through processes of shallow subduction resulting in a near-horizontal mantle stratigraphy (i.e., H, X) both compositional and rheological in nature. Interpretation of L as the continuation of dipping reflectors on the seismic reflection profile argues for a final phase of craton assembly involving oblique underplating of subducted lithosphere in the Proterozoic. Subsequent modification of the lithosphere, as manifest by Phanerozoic kimberlite volcanism, may be related to W if an interpretation as the top of a layer containing a dense silicate melt fraction is invoked.

1. Introduction

Elucidation of the mechanisms controlling the stabilization of continents poses one of the outstanding challenges in Earth science. The Archean provinces that core continents are of particular interest because the processes leading to their assembly may have been significantly modified or are no longer operative in more recent times [e.g., *Bickle*, 1986; *Abbott*, 1991]. Advances in our understanding of continental evolution have been hindered, in part, by the inaccessibility of the mantle component of the continental lithosphere. Indeed, access to the subcrustal lithosphere is generally restricted to the large-scale remote sensing afforded by long-period seismology, and local sampling of xenoliths entrained within kimberlites and alkaline basalts. The correlation of exposed Precambrian shields with long-wavelength, high-velocity anomalies in the shallow (50-300 km) upper mantle as revealed through seismic studies [e.g., *Grand*, 1994], requires that the mantle lithosphere play a prominent role in the stability and evolution of continents [e.g., *Jordan*, 1978, 1988]. However, the detailed structure of the continental "roots" and their development are still poorly understood. Important information on age [e.g., *Richardson et al.*, 1984; *Pearson et al.*, 1995], composition [e.g. *Boyd*, 1989], and fabric [e.g., *Mainprice and Silver*, 1993] has come from the analysis of the deep-seated xenoliths erupted in kimberlites which represent our deepest direct sampling of the Earth's interior [*Boyd and Gurney*, 1986; *Haggerty and Sautter*, 1990]. These studies identify a compositional signature to the roots and suggest they formed synchronously with or soon after stabilization of overlying crust. The sampling of kimberlites is, however, restricted and local, and it is not generally known to what extent erupted xenoliths (1) are representative of typical Archean mantle and (2) have been modified in the eruption process [*Harte and Hawkesworth*, 1989]. There is thus a need for strategies which permit the interrogation of the continental mantle at finer-scales than generally possible with long-period seismology and which

Paper number 98JB01069.
0148-0227/98/98JB-01069$09.00

are not subject to the sampling vagaries of intraplate volcanism.

The analysis of converted seismic phases has proven useful in detailed characterization of both the crust [e.g., *Langston,* 1979; *Owens et al.*, 1987; *Cassidy*, 1995] and the mantle transition zone [*Vinnik*, 1977; *Shearer*, 1991]; however, application to the lithospheric mantle has been exacerbated by the presence of prominent crustal reverberations which coincide temporally with direct mantle conversions [*Bostock*, 1996]. The objective of the present work is two fold: (1) to demonstrate that through systematic analysis of large quantities of 3-component broadband teleseismic data it is possible to extract detailed information on mantle lithospheric stratigraphy and (2) to apply this approach to a data set collected at Yellowknife, Northwest Territories, to gain insight into processes effecting the evolution of the Archean Slave province in the northwestern Canadian Shield.

2. Tectonic Setting

The city of Yellowknife and the Yellowknife Array (hereinafter YKA) sit near the southern terminus of the Slave province (hereinafter the "Slave"), an Archean granite-greenstone block located in the northwestern Canadian shield (Figure 1). The history of the Slave encompasses an interval of 4.0 Ga extending back to formation of the Acasta gneiss [*Bowring et al.*, 1989] in the western Anton terrane. The Anton terrane is interpreted as the remains of a larger Archean continent or microcontinent which accreted, through eastward subduction, to a younger, paired accretionary prism and island arc, now constituting the eastern Slave, at 2.6 Ga [*Kusky*, 1989]. Rocks to the east of the inferred suture are everywhere less than 2.8 Ga. Geochemical evidence from Pb [*Thorpe et al.*, 1992] and Nd [*Davis and Hegner*, 1992] isotope studies further indicate a fundamental division between the eastern and western portions of the Slave. Yellowknife and the YKA are situated near the eastern boundary of the Anton terrane and lie some 100-150 km north of the Great Slave Lake shear zone (GSLsz) and a comparable distance east of the Proterozoic Wopmay orogen. The GSLsz is interpreted as a 1300 km long, 1.9 Ga intracontinental transform fault resulting from eastward indentation of the Slave into the (largely reworked) Archean Churchill province [*Hoffman*, 1987]. The Wopmay orogen borders the western margin of the Slave and represents a complex history of early (1.97 Ga) rifting, collision with the Hottah terrane through westward subduction (1.97-1.885 Ga), initiation of eastward subduction and development of the Great Bear magmatic arc [*Hoffman*, 1980; *Bowring and Grotzinger*, 1992], and finally docking of the Fort Simpson terrane near 1.84 Ga [*Villeneuve et al.*, 1991].

3. Data Set

The YKA was originally installed by the British Ministry of Defence in 1962 and has operated since that time under the auspices of the Geological Survey of Canada. In late 1989, equipment was upgraded to allow digital recording of broadband signals at four stations, YKW1-4, within the larger short-period array. In addition, the U.S. Department of Energy deployed one of the Regional Seismic Treaty Network stations, RSNT, at the site over the period 1983-1986 [*Owens et al.*, 1987]. This history of broadband recording is complemented by an optimal location with respect to global seismicity. Figure 2 shows the distribution of the 460 events used in this study. Two narrow azimuthal corridors associated with the western Pacific and Latin American subduction zones provide excellent sampling in epicentral distance, while azimuthal coverage is significantly lacking only to SW and ENE azimuths. The multiplicity of stations has resulted in a total of 1033 broadband three-component seismograms available to this study.

4. Methodology

Analysis of the large number of seismograms collected here is facilitated by normalization of source signature to isolate features related to the structural response of the Earth. The approach employed in this study is similar to receiver function analysis commonly used in crustal studies [e.g., *Langston*, 1979] but incorporates a number of important modifications to enhance subtle features arriving at later times in the wave train; these are outlined briefly below.

The success of receiver function analysis results from the fact that most of the near-receiver P-S converted energy in the teleseismic P wave coda resides on the radial component whereas P wave energy is confined primarily to the vertical component. The P contribution to the impulse response is considerably simpler than that of S as it more nearly coincides with a delta function, and so the vertical component seismogram can be used as an effective approximation to the source time function. Deconvolution of the vertical component from the radial component therefore results in a reasonable approximation to the S wave response, one which can be improved upon by considering a more accurate wave field decomposition. At the Earth's free surface ($z = 0$), the zero traction boundary condition allows one to relate the rotated ground displacement vector $\mathbf{u} = [U_R, U_T, U_Z]^T$ to the upgoing wave field $\mathbf{w} = [P, SV, SH]^T$ through a transfer matrix $\mathbf{M}$ as

$$\mathbf{u}(0) = \mathbf{M}\mathbf{w}(0), \tag{1}$$

where all quantities are expressed in the frequency-slowness (ω, p) domain, and $\mathbf{M}$ is derived from the partitions of the fundamental matrix of elastic wave propagation in horizontally stratified media evaluated at the Earth's surface [see, e.g., *Kennett*, 1983]. In isotropic media, this 3×3 matrix relation is decoupled into a 2×2 equation describing $P - SV$ motion and a scalar relation for SH motion. *Kennett* [1991] has shown how the elements of $\mathbf{M}^{-1}$ in an isotropic medium can be expressed in simple analytic forms which involve the surface compressional and shear velocities α, β, density ρ, and slowness p. The explicit relation is

$$\begin{pmatrix} P \\ SV \\ SH \end{pmatrix} = \begin{pmatrix} p\beta^2/\alpha & 0 & \frac{\beta^2 p^2 - \frac{1}{2}}{\alpha q_\alpha} \\ \frac{\frac{1}{2} - \beta^2 p^2}{\beta q_\beta} & 0 & p\beta \\ 0 & \frac{1}{2} & 0 \end{pmatrix} \begin{pmatrix} U_R \\ U_T \\ U_Z \end{pmatrix}, \tag{2}$$

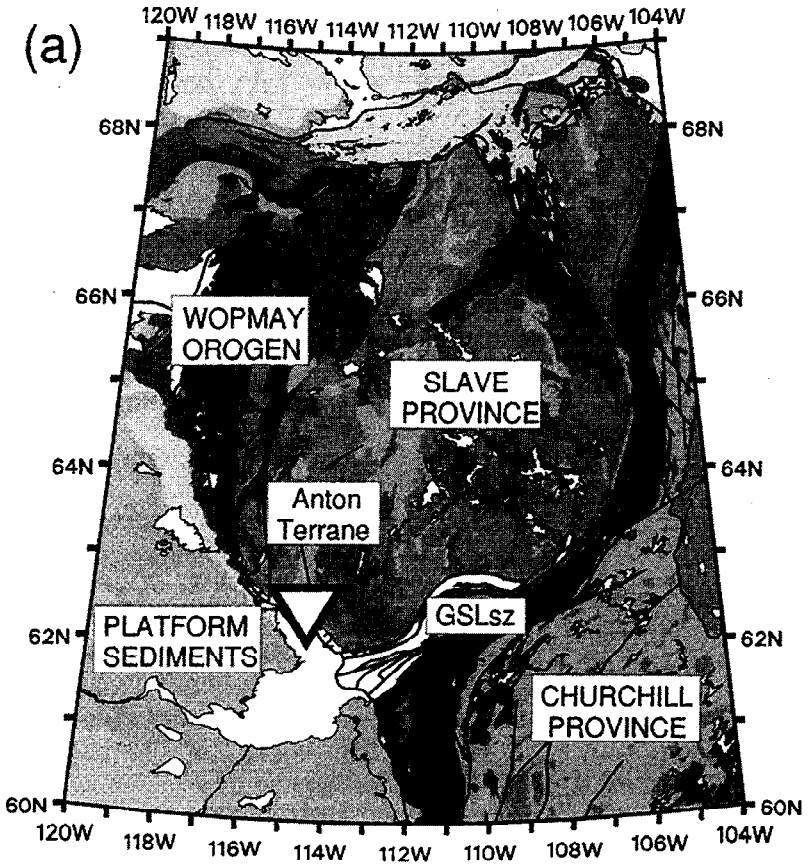

Figure 1. Study location. (a) Generalized geological map of the Slave province showing location of major tectonic features and the YKA (inverted triangle). (b) Detailed map of Yellowknife area showing locations of five stations used in this study.

where $q_\alpha = \sqrt{\alpha^{-2} - p^2}$ and $q_\beta = \sqrt{\beta^{-2} - p^2}$. Over the slowness band corresponding to teleseismic P waves, the expressions are slowly varying and so an exact knowledge of the near-surface physical parameters is not critical.

This wave theoretic approach may be further extended to aid in the suppression of free surface multiples from the Mohorovicic discontinuity (hereinafter M) which present a major impediment to interpretation. Application of a multiple suppression operator to the wave field recorded at the free surface yields the dereverberated data as [*Kennett*, 1991]

$$\mathbf{T}_U \mathbf{w}(z_M) = \left(\mathbf{I} - \mathbf{R}_D \widetilde{\mathbf{R}}\right) \mathbf{w}(0), \qquad (3)$$

where z_M is the depth corresponding to the base of the crust, $\mathbf{T}_U$, $\mathbf{R}_D$ are the upward transmission and downward reflection matrices characterizing the crustal column, and $\widetilde{\mathbf{R}}$ is the free-surface reflection matrix. Practical considerations restrict implementation to one-dimensional (1-D) Earth models which nevertheless require accurate estimates of crustal velocities and density for effective multiple suppression. For this reason, (3) is generally less useful than (2).

Once wave field decomposition (and multiple suppression, if applied) is complete, the P wave is windowed in the time domain to avoid wrap-around effects in deconvolution and to exclude energy judged not to contribute significantly to the source time function. In particular, it is useful to monitor the timing of the phase PP, which because of significantly greater slowness at nearer offsets (i.e., 30°-50°), causes degradation in the deconvolution if it is not removed. Depending on the particular purpose, deconvolution will often involve the collection of several wave field-decomposed seismograms to estimate a single impulse response $g(t)$, and it is generally expedient to perform least squares simultane-

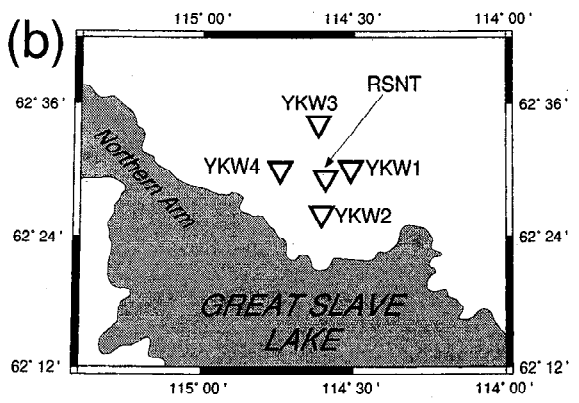

Figure 1. (continued)

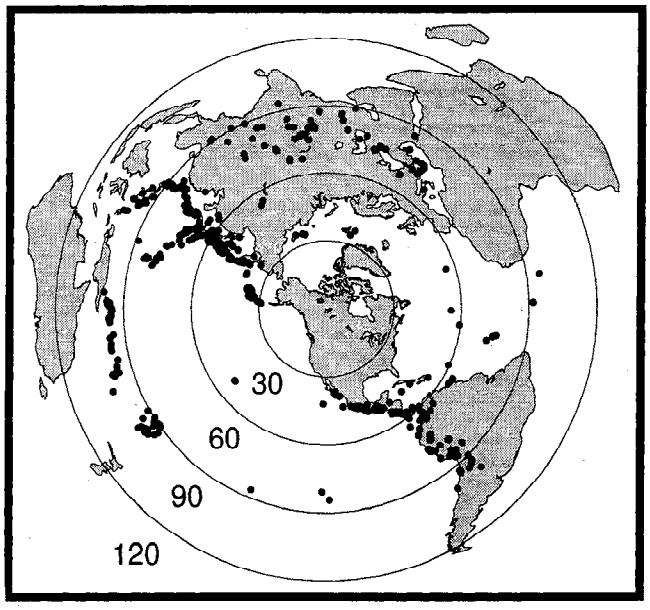

Figure 2. Azimuthal projection centered on YKA showing distribution of events used in this study and recorded over the periods 1983-1986 and 1990-1997. Small circles mark epicentral distances of 30°, 60°, 90° and 120° from YKA.

ous deconvolution of all N seismograms in the frequency domain [*Gurrola et al.*, 1995] as

$$g(t) = \mathcal{F}^{-1}[G(\omega)] = \mathcal{F}^{-1}\left[\frac{\sum_n^N S_n(\omega)P_n^*(\omega)}{\sum_n^N P_n(\omega)P_n^*(\omega)+\delta}\right], \quad (4)$$

where S_n represents the S wave component under consideration (either SV or SH) from the nth seismogram, P_n is the corresponding windowed P wave component, $\mathcal{F}^{-1}$ denotes inverse Fourier transformation, asterisk denotes complex conjugate, and δ is a regularization parameter which controls the trade-off between model variance and data misfit. The optimum δ-parameter is chosen by minimizing the general cross validation function $GCV(\delta)$ [*Golub et al.*, 1979], which, in frequency domain deconvolution, may be shown to equal

$$GCV(\delta) = \frac{\sum_n^N \sum_m^M \left(S_n(\omega_m) - P_n(\omega_m)G(\omega_m)\right)^2}{\left(NM - \sum_m^M X(\omega_m)\right)^2}, \quad (5)$$

where

$$X(\omega) = \frac{\sum_n^N P_n(\omega)P_n^*(\omega)}{\sum_n^N P_n(\omega)P_n^*(\omega)+\delta}, \quad (6)$$

and M is the number of frequencies represented in the discrete Fourier transform. This choice of estimate for δ results in a model $G(\omega)$ which, in a sense, optimally predicts the data $S_n(\omega)$ and holds the advantage that no assumptions are made regarding noise levels in the data [cf. *Oldenburg*, 1981].

Simultaneous deconvolution of seismograms along moveout curves as required, for example, to map energy in stacks of converted phases into mantle "reflectivity" $R(z)$ is accomplished through the inclusion of phase delays in the numerator of the expression in (4) as

$$R(z) = \mathcal{F}^{-1}\left[\frac{\sum_n^N S_n(\omega)P_n^*(\omega)\exp(i\omega\tau(p_n,z))}{\sum_n^N P_n(\omega)P_n^*(\omega)+\delta}\right], \quad (7)$$

where $\tau(p_n, z)$ is the delay time of a converted phase originating at an interface at depth z in the mantle, and p_n is the horizontal slowness associated with the P wave of the nth seismogram.

5. Mantle Stratigraphy

Prior to the presentation of results, several important properties of near-receiver converted phases pertinent to subsequent interpretation are reviewed. Theoretical travel times from a 1-D Earth model (derived for data described later in this section), for a number of phases resulting from horizontal planar discontinuities and relevant to the ensuing discussion, are shown in Figure 3a plotted relative to the arrival of direct P. The direct Ps conversion from M is designated P_Ms at $\sim$ 5 s (henceforth converted phases originating at a discontinuity D will be referred to as P_Ds, see Figure 3b)

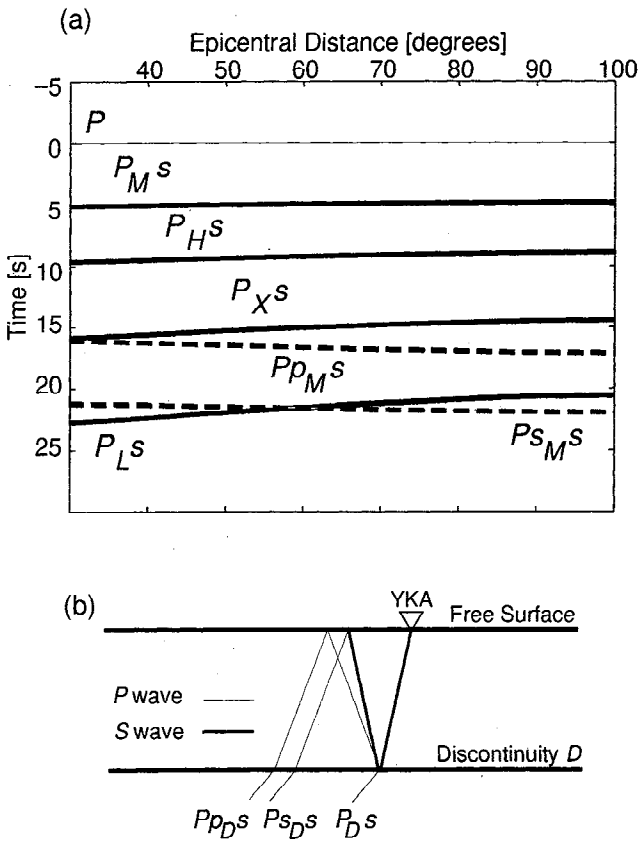

Figure 3. (a) Theoretical travel times of P to S converted phases between -5 and 25 s after the arrival of direct P. Direct P_Ds conversions are shown in solid lines, and crustal reverberations are shown in dashed lines. (b) Schematic diagram illustrating geometry of phases shown in Figure 3a for a generic discontinuity D.

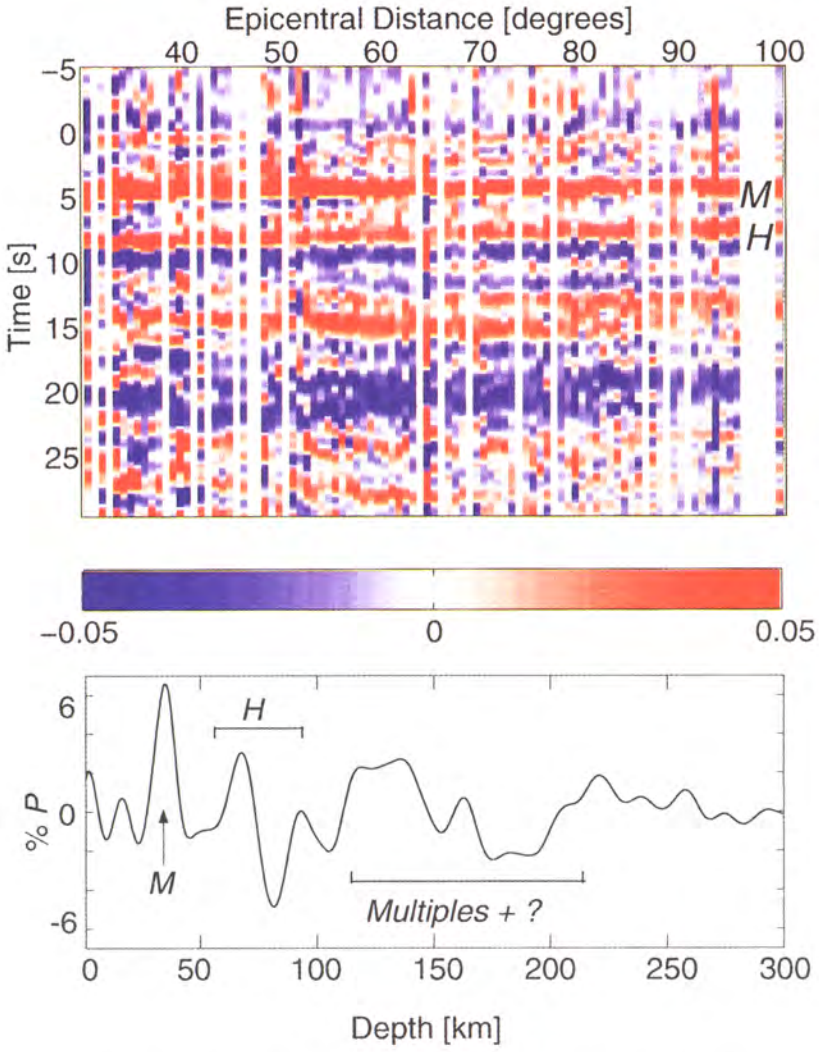

Plate 1. Radial (SV) impulse response from NW (274°-313°) corridor between -5 and 25 s after direct P. (top) Color-coded impulse responses for a range of epicentral distances. (bottom) Mapping of the same seismogram data set to depth. Responses are filtered between 0.75 and 0.04 Hz. Signatures of M and H are marked.

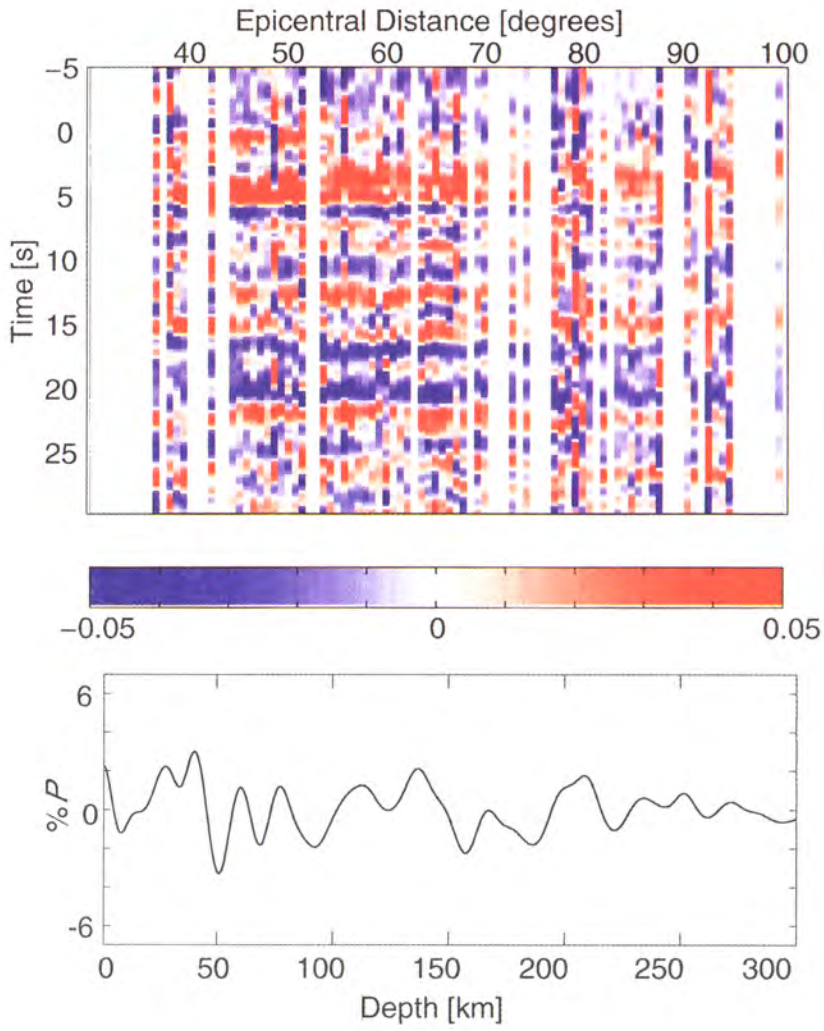

Plate 2. Radial (SV) impulse response from SE (131°-181°) corridor between -5 and 25 s after direct P. Description as for Plate 1.

while the two most significant (i.e., first order in reflection or conversion coefficient) free-surface reverberations, $Pp_{M}s$ and $Ps_{M}s$ (in dashed lines) follow at approximately 16 and 21 s, respectively. An important property of direct conversions is that they exhibit negative differential slowness with respect to direct P which distinguishes them from reverberations. This property persists for inclined layers at a range of dip angles. A second consideration involves the spatial sampling of the converted phases, both geometric and from the point of view of finite bandwidth. Figure 4 illustrates the horizontal distance between conversion point and receiver as a function of boundary depth for a range of slownesses relevant to this study. Here it is apparent that the horizontal distance traveled is of the order of one third the depth of origin. A further averaging of the wave due to finite bandwidth is expressed through the concept of Fresnel zones. The Fresnel zone will depend on the dominant frequencies and depth to interface. Assuming that constructive interference arises for phase differences less than a quarter period, the diameter of the Fresnel zone varies between $\sim$ 25 km for $P_{M}s$ at 0.5 Hz to $\sim$ 160 km for $P_{660}s$ (generated at the 660 km discontinuity) at 0.25 Hz.

5.1. Mohorovicic Discontinuity

In this section we examine and review characteristics of the M at YKA relevant to the interpretation of deeper structures. The impulse response for SV from western Pacific and South American azimuthal corridors (compare Figure 2) is shown in Plates 1 and 2 between -5 and 25 s after direct P. The bottom panel in both plates shows the same data mapped to depth as an expression of mantle "reflectivity". This is accomplished by simultaneously deconvolving all seismograms along moveout curves for converted phases originating at a regularly sampled series of depths in a 1-D Earth model, followed by interpolation along the expected time-depth trajectory (see (7)). Care must be taken in interpreting these panels since the presence of free-surface crustal multiples clearly violates the assumption that all energy results from $P_{D}s$ conversions generated at horizontal discontinuities.

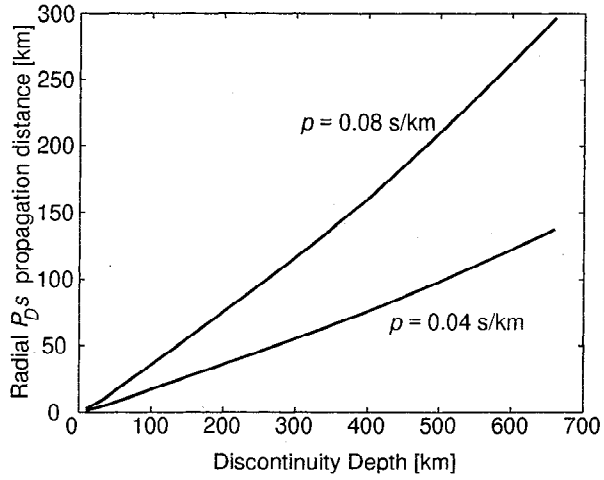

Figure 4. Horizontal conversion distance as a function of conversion depth for $P_{D}s$ phases determined for a typical 1-D Earth model.

The time interval 0-25 s corresponds to direct $P_{D}s$ conversions arriving from discontinuities between 0 and 250 km depth. $P_{M}s$ is evident in both plots as a positive polarity (red) streak at $\sim$ 4.5 – 5 s after P. As noted by *Cassidy* [1995], the crustal stratigraphy at YKA shows significant variations from different azimuths, with impulse responses from the NW and N being most simple [*Owens et al.*, 1987]. The results here corroborate these observations, and show a simple, single-peaked $P_{M}s$ over the entire epicentral distance range for the NW corridor with amplitude $\sim$ 6% that of P (hereinafter all quoted amplitudes are with respect to direct P). A single-layer crustal model of P and S velocities 6.5 and 3.7 km/s and thickness 36.5 km suffices to explain the travel times of $P_{M}s$ and $Pp_{M}s$ (Figure 5). The impulse responses to the SE, in contrast, are weaker (3-4%), double peaked (3.5 and 5 s), and exhibit a more prominent negative polarity loop at 5.5 s. Strong variations in the observed travel time curves from this azimuth render crustal structure more difficult to model in one dimension, but the later $P_{M}s$ time suggests a deeper M consistent with an early refraction study where the thickness of the crust was observed to increase along a profile oriented NW-SE across the east arm of Great Slave Lake and GSLsz [*Barr*, 1971].

Images of stratigraphy (including M) as functions of back azimuth and depth are shown in Plate 3. Impulse responses for each individual azimuthal bin have been constructed as the lower panels in Plates 1 and 2. The images may thus be likened to projections of Earth structure along a vertically oriented, conical sheet with apex at the surface recording station. Note that some spatial averaging results from the inclusion of data from five stations (Figure 1b). The SV component image suggests a slight increase in depth and more complicated structure of M 10-20 km to the SSE of YKA. There is little expression of $P_{M}s$ on the transverse component with amplitudes generally less than 2% over most of the back azimuthal range. This is an observation with important consequences for analysis of deeper structures. It indicates that, although some crustal heterogeneity (and possibly anisotropy in the subjacent mantle) exists, its expression is insufficient to produce strong amplitudes on the SH component.

5.2. Mantle Lithosphere

Analysis of subcrustal discontinuities using SV impulse responses is complicated by the presence of the two crustal multiples $Pp_{M}s$, $Ps_{M}s$ which effectively mask the time interval at which direct $P_{D}s$ phases originating at depths between approximately 130-210 km would arrive. An examination of Plate 1 indicates that, prior to the arrival of these multiples, a well-defined phase which we label $P_{H}s$ (H references the Hales [1969] discontinuity), is apparent between 8 and 10 s with a distinctive double-lobed character (sequential positive and negative peaks) and negative differential slowness which identifies it as a direct $P_{D}s$ conversion. This feature is still better defined on SH for the NW corridor (see Plate 4) where it exhibits the same polar-

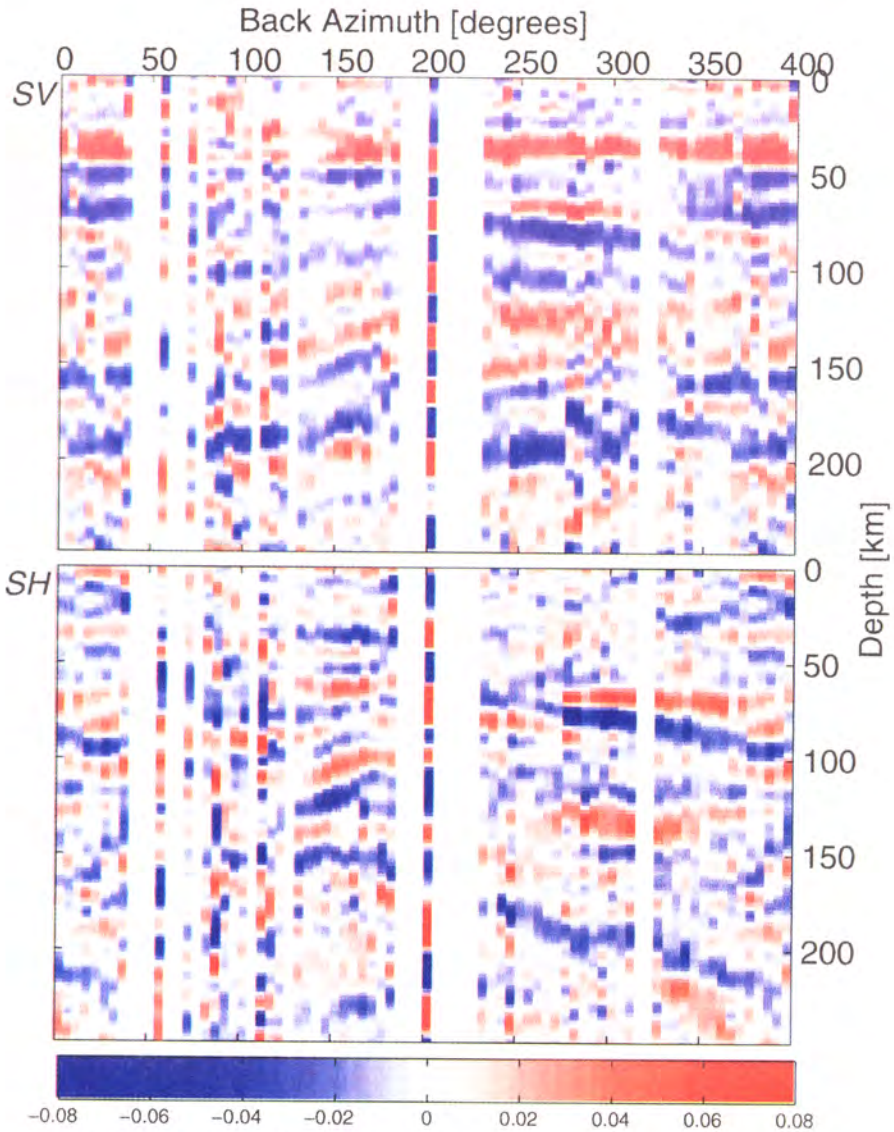

Plate 3. Radial (SV) and transverse (SH) impulse responses mapped to death as a function of back azimuth at YKA. M, at 35-40 km depth, produces misstacked reverberations which contaminate the SV response. The absence of significant M on the SH affords a window into the mantle where H, X, and L are clearly visible. Note that deeper discontinuities are sampled at greater lateral distances from YKA than shallow ones (figure 4), and so profiles can be viewed as slices through the Earth along a conical surface with vertical axis and focus at YKA.

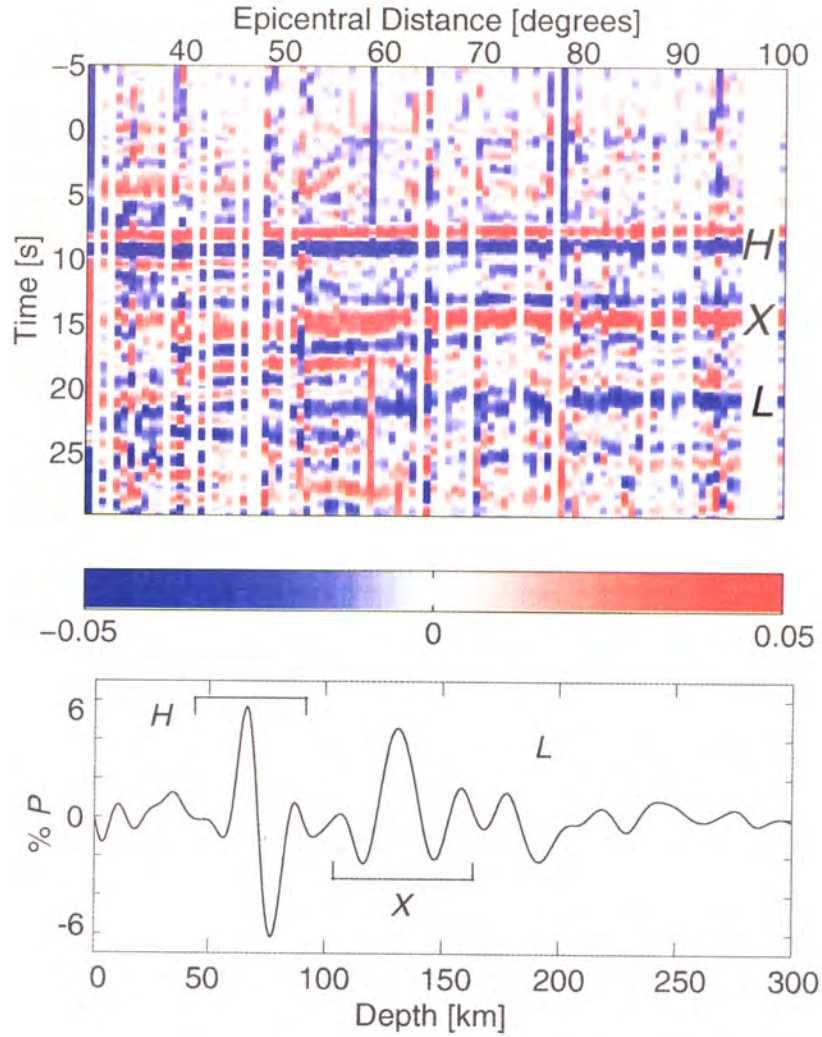

Plate 4. Transverse (SH) impulse response from NW (274°-313°) corridor between -5 and 25 s after direct P. Description as for Plate 1. Signatures of H, X, and L are marked.

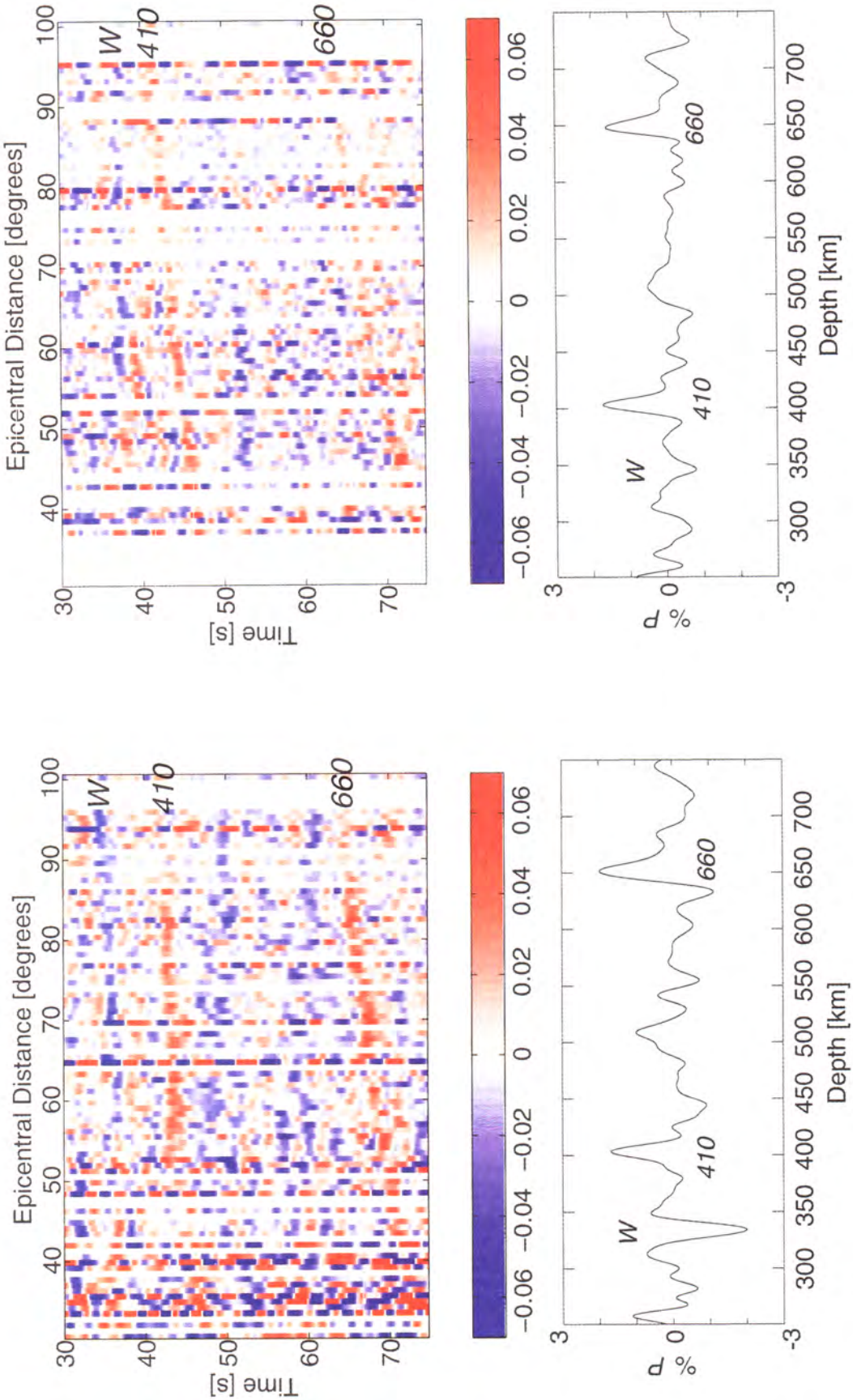

Plate 5. Radial (*SV*) impulse response from NW (274°-313°) corridor between 30 and 75 s after direct *P*. Description as for Plate 1. Signatures of *W* and the 410 and 660 km discontinuities are marked.

Plate 6. Radial (*SV*) impulse response from SE (131°-181°) corridor. Description as for Plate 1. Signatures of *W* and the 410 and 660 km discontinuities are marked.

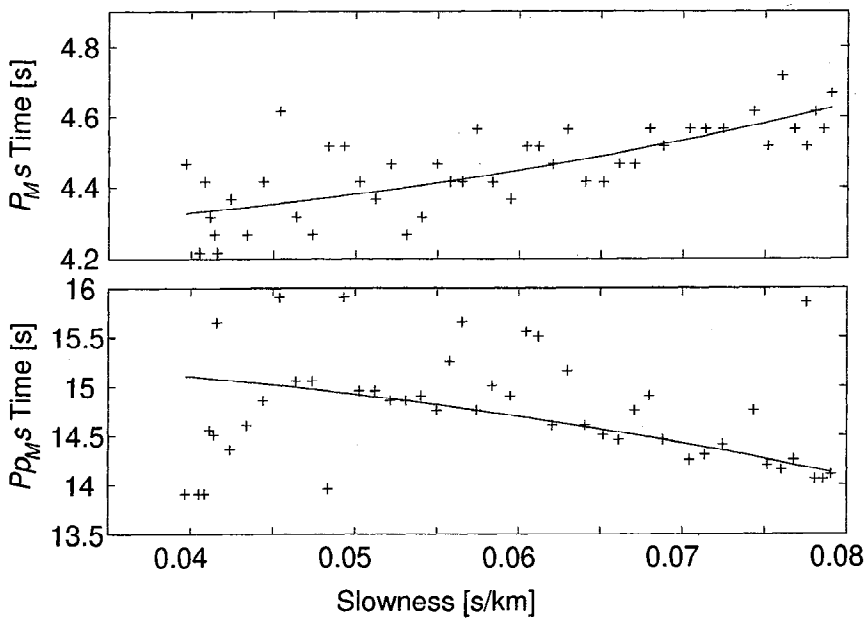

Figure 5. Inversion of $P_M s$ and $Pp_M s$ travel times for crustal parameters along the NW corridor. Observed travel times (shown as pluses, and determined from the amplitude maxima between 4 and 6 s in Figure 5) are reasonably described by 36.5 km thick crustal layer with P and Svelocities of 6.5 and 3.7 km/s, respectively.

ity and larger amplitude. The first peak is characterized by higher frequencies than the second with significant energy to frequencies of at least 3 Hz. Two other phases with negative slowness and laterally coherent amplitude are obvious in Figure 4 at times of approximately 15 and 21 s, respectively, which, because of strong amplitudes on the SH component, are not significantly contaminated by crustal multiples. The first of these, labeled as $P_X s$ (centered at approximately 135 km depth with amplitude 4-5%), consists of broad positive pulse bracketed by two higher frequency negative loops, while the second, $P_L s$, (near 190 km depth, amplitude $\sim$ 3%; L references the Lehmann [1961] discontinuity) is a generally lower frequency, single, negative peak.

Significant energy levels on the SH impulse responses manifest the presence of lateral heterogeneity, anisotropy, or some combination thereof. $P_H s$ is the best defined of the features outlined above and, owing to its proximity to the surface, is sampled over the smallest region (compare Figure 4). The double-lobed character is most easily modeled through the generation of P-S conversions at the boundaries of a layer $\sim$ 10 km thick located between $\sim$ 70 and 80 km depth. The behavior of $P_H s$ as a function of back azimuth on the SV component in Plate 3 indicates a polarity cross over near 320°. Equivalently, the layer appears as high velocity from azimuths between 230° and 320°, whereas between 320° and 400° (40°) back azimuth it appears to be characterized by lower velocities. On the SH component, polarity cross overs occur near 270° and 180° (most obvious in individual station responses from YKW1 and YKW3) back azimuth, and it is apparent here that the large amplitudes observed in Plate 1 are confined to a narrow azimuthal range. Taken together, these observations support an explanation in terms of anisotropy since simple lateral heterogeneity (i.e., in the form of dipping layers) alone should not yield polarity cross overs on the SV component and further should give rise to 360° periodicity (i.e., 180° polarity cross overs) on the SH component. It is worth noting, however, that the amplitude behavior is complicated; the phase is best defined from northern azimuths (in particular, between 275° and 313° on the SH component) and becomes weaker to the south at the expense of energy arriving immediately after $P_M s$. It is difficult to model this behaviour with 1-D models, as shown in a later section, even when considering the range of slownesses represented in the data, and so it is likely that lateral heterogeneity also contributes to the signal.

It is more difficult to characterize the structures responsible for $P_X s$ and $P_L s$ because of the crustal multiples present on the SV component, and because they sample larger areas with a consequent increased susceptibility to the influence of lateral heterogeneity. Some success was achieved in suppression of multiples using the dereverberation operator in equation (3). Crustal thickness, velocity, and density were estimated using the inversion results of Figure 5 for a homogeneous crustal model, and a similar inversion of $P_M s$, $Pp_M s$ amplitudes constrained jumps in shear velocity and density across M at z_M. $P_X s$ becomes more clearly defined on SV and appears on both components between 270° and 360° back azimuth, deteriorating to the NE. It is not clear how it evolves across the data gap to the SW into the back azimuthal corridor represented by the Latin American subduction zones. Both polarity reversal and variations due to lateral heterogeneity likely occur. In contrast to H it is dif-

ficult to model this feature by anything less than two layers (see later section on reflectivity synthetics).

P_Ls is the last, laterally coherent feature apparent on the SH component. It consists primarily of a single negative peak, although there is some suggestion of associated deeper, but weaker, structure between 330° and 360° back azimuth in Plate 3 and in Plate 4. The feature is continuous and unique polarity between 250° and 400°(40°) back azimuth and apparently increases in depth from $\sim$ 170 km depth in the west to $\sim$ 230 km to the NE. The general consistency of $P_{410}s$ [*Bostock and Cassidy*, 1997] and shallow mantle P_Ds travel times from all azimuths indicates this depth increase is real and not the result of lateral velocity variations. Absence of polarity cross over in $\sim$ 150° of back azimuth and the observed dip suggest that the appearance of P_Ls on the SH component is, at least in part, due to lateral heterogeneity, and that L is being sampled to one side of the dip vector. Further, a careful examination of the dereverberated SV component, following (3), reveals a positive velocity contrast for L, again consistent with the observed dip.

5.3. Asthenosphere and Transition Zone

Significant energy after P_Ls is confined primarily to the SV component impulse responses and occurs at times ($>$ 23 s) when interference with crustal reverberations is no longer a concern. Along the NW corridor, the most prominent feature in the interval between 25 and 40 s is a negative polarity arrival which can be traced across the entire epicentral distance range and stands out clearly on the summary depth profile in Plate 5. It is characterized by a timing and slowness that identify it as a P_Ds conversion from a negative velocity contrast interface near 335 km depth (hereinafter referred to as W [*Revenaugh and Sipkin* 1994]), and includes energy to higher frequencies (0.5 Hz) than $P_{410}s$ that succeeds it by $\sim$ 7 s. A similar arrival is also apparent from the SE (Plate 6), and, although less well defined, appears to originate at slightly greater depth (350 km). The observed differential slowness from this azimuth is less negative than that expected for a horizontal interface at 350 km depth such that it does not stack optimally in the depth profile of Plate 6. This is apparently the result of topography, and an alternative explanation as a reverberation can be discounted on several grounds: (1) the slowness is slightly negative (see top panel Plate 6); (2) P_Ws from the NW and the feature to the SE would appear to be one and the same and the slowness of the former clearly conforms with that expected for a direct conversion; (3) Pp_Hs and Pp_Xs, the most likely candidate phases, would be expected at times of $\sim$ 28 s and $\sim$ 47 s, respectively; (4) there is no indication of coherent energy on the SH component nor does P_Ws show evidence for a multilobed signature; (5) a diffuse Pp_Xs is visible in Plate 6 and has clearly suffered attenuation of high frequencies from two extra legs through the lithosphere while P_{350s} from the SE maintains a high-frequency signature.

The transition zone beneath YKA, as revealed by Ps conversions, has been studied by a number of authors [*Stammler et al.*, 1992; *Petersen et al.*, 1993; *Bostock and Cassidy*, 1997] and so will not be considered in detail here. Prominent $P_{410}s$ and $P_{660}s$ phases are evident on SV component impulse response functions from both NW and SE azimuths (Plates 5 and 6). Both show up clearly on the SV summary depth profiles with comparable amplitudes near 2%. Amplitudes on the SH components at similar times are low ($<$ 1%), but superposition of SH and SV components shows evidence of the time-derivative relationship expected for shear wave birefringence through a homogenous, anisotropic layer [e.g., *Kind et al.*, 1985]. This attests to the relative efficiency of mode conversion at anisotropic interfaces in generating energy on the SH component as observed, for example, in P_Hs, P_Xs. Radial profiles from both the NW and SE corridors also suggest broader but coincident energy peaks near 510 km depth perhaps signaling conversion of lower frequency energy from an extended "520" km discontinuity [*Shearer*, 1991; *Bostock*, 1996].

6. P_Ds Synthetic Seismograms

In this section, synthetic seismograms are presented for anisotropic media using an implementation [*Martin and Thomson*, 1997] of the reflectivity method of *Kennett* [1983]. The purpose is to demonstrate a number of phenomena associated with P_Ds conversions in anisotropic media that are represented in the data and relevant to their interpretation. For a more comprehensive treatment, the reader is referred to *Levin and Park* [1997]. Radial and transverse seismograms (p = 0.06 s/km), are shown in Figure 6 as a function of back azimuth for three simple models. Crustal reverberations are not included in the synthetics for the sake of clarity. Each model comprises an isotropic crust, overlying a sequence of three alternating isotropic/anisotropic layers of varying thickness (see Table 1 for details). The anisotropic layers (3 5 7) are modeled with orthorhombic symmetry using a scheme detailed by *Martin and Thomson* [1997] such that they result in ±5% velocity anisotropy for qP and vertically propagating qS waves. The orientation of anisotropy in layer 3 (broadly meant to represent H) in the top panel is such that the a axis aligns E-W, the b axis is aligned vertically, and the c axis aligns N-S and is thus configured with a horizontal mirror symmetry plane (note here that a, b, and c represent the fast, slow, and intermediate axes, respectively). In the bottom two panels this orientation is modified such that for panel 2 the $a-b$ plane has been rotated 60° clockwise about the c axis, and for panel 3 the $b-c$ plane has been rotated 60° clockwise about the a axis. The orientation of anisotropy in layers 5 7 (collectively with 6, meant to represent X) remains constant in all three panels and is similar to that for layer 3, panel 1 except that the $a-c$ plane has been rotated about the b axis by 45° and 135°, respectively.

All anisotropic layers in the top panel thus possess horizontal mirror symmetry with the result that the SV image is symmetric about 0° (or 180°), whereas the transverse image is antisymmetric. P_Ms is obvious as a continuous positive peak at $\sim$ 4.5 s restricted to the SV component. In contrast, P_Hs is clearly evident on both SV and SH plots as a dipolar pulse between 8 and 10 s exhibiting a 180° peri-

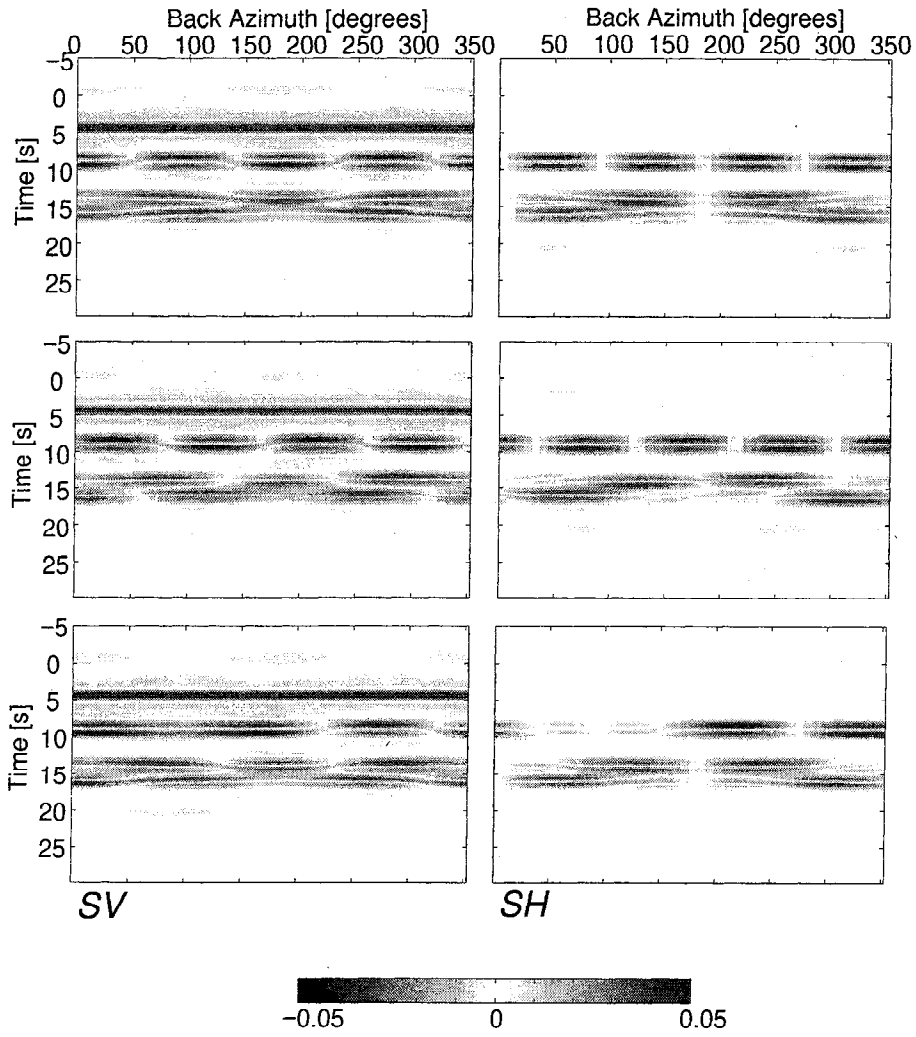

Figure 6. Synthetic P_{Ds} seismograms. Panels in right (left) column are SV (SH) impulse responses as functions of azimuth for the three models of upper mantle anisotropy described in text and in Table 1. Note that units are different from Figure 8 in that these traces have not been mapped to depth. A qualitative comparison may be made as the mapping causes negligible waveform distortion.

odicity in back azimuth. The deeper layer sequence (5 6 7) produces a more complex signal due to interference of conversions which reproduces some of the character witnessed for $P_X s$ in the data (Plate 4), notably the appearance of a broader positive peak flanked by two narrow negative pulses between 250° − 300° back azimuth. This effect could not be attained with anything less than two layers with the three-layer configuration furnishing the best empirical fit. The

Table 1. Model Parameters for Synthetic Seismograms.

Layer	Interval, km	$\overline{\alpha}$, km/s	$\overline{\beta}$, km/s	ρ, kg/m^3	Elasticity
1	0.0-36.5	6.54	3.71	2600	isotropic
2	36.5-74.5	8.10	4.50	3500	isotropic
3	74.5-84.5	8.10	4.50	3500	anisotropic
4	84.5-124.5	8.10	4.50	3500	isotropic
5	124.5-129.5	8.10	4.50	3500	anisotropic
6	129.5-144.5	8.10	4.50	3500	isotropic
7	144.5-149.5	8.10	4.50	3500	anisotropic
8	149.5-∞	8.10	4.50	3500	Isotropic

Variables $\overline{\alpha}$, $\overline{\beta}$ refer to average velocities for anisotropic layers. Anisotropic layers 3 5 7 are modelled with orthorhomic symmetry using the scheme of *Martin and Thomson* [1997] and represent ±5.5% velocity anisotropy for both P and vertically propagating S waves. The orientation of anisotropy for layers 5 and 7 is kept fixed with $\theta_a = 45°, 135°$, respectively. See text for details on layer 3.

picture is modified slightly in the central panel where H no longer possesses horizontal mirror symmetry. The primary effect on P_Hs is a rotation of the signature by $\sim 45°$ while the 180° azimuthal periodicity is maintained. In contrast, the waveform of P_Xs is more severely distorted. In the bottom panel anisotropy in H once more deviates from horizontal symmetry but now through rotation about the other horizontal axis. The effect is markedly different; P_Hs now displays a combination of 180° and 360° periodicity in back azimuth, as noted previously by *Levin and Park* [1997], which results in substantially reduced amplitudes between 40° and 160° back azimuth. Furthermore, P_Xs shows very little difference from that in the top panel. The contrasting behavior in the two bottom panels manifests the different response to this form of orthorhombic anisotropy by qP and qS modes and underlines the possibility that P_Ds signatures from deeper interfaces may suffer significant distortion from more shallow layering.

7. Discussion

Attention is now directed toward the tectonic and geodynamic significance of features responsible for the P_Ds conversions identified in previous sections. The structure which we have termed H (thereby maintaining consistency with previous studies that have identified discontinuities at similar depths [e.g., *Zandt and Randall*, 1985; *Revenaugh and Jordan*, 1991]) possesses four distinct attributes which must be accommodated by any mechanism of origin: (1) layer thickness $\sim$ 10 km; (2) strong, localized anisotropy; (3) average velocity comparable to that of the ambient mantle; and (4) sharp boundaries, in particular, the teleseismic data dictate a transition of less than 700 m for the upper interface.

The consensus that has emerged from previous work [e.g., *Revenaugh and Jordan*, 1991] is that the mantle velocity increase occasionally observed between 50 and 100 km depth in both continental and oceanic environments is best ascribed to the transition from spinel to garnet in aluminous peridotite [*O'Neil*, 1981]. This mechanism can be forced to accommodate the present observation of H if appeal is made to transformation plasticity [e.g., *Sammis and Dein*, 1974; *Poirier*, 1982] as a means of rheologically weakening the phase transition depth interval, causing volumetric strain, and thereby possibly permitting development of anisotropic fabric. *Webb and Wood* [1986] report transition intervals of 6 km for the spinel to garnet phase change in naturally occurring peridotites which is consistent with thickness of H observed here after making allowance for possible compositional effects. However, the absence of obvious deformation in lherzolite xenoliths within the phase transition interval from the Slave (as revealed in thin section where a simple coronal replacement of garnet by spinel is observed (M. Kopylova, personal communication, 1997)) and the sharp upper boundary of H would appear to render an origin in the spinel→garnet phase transition unlikely. If the condition of an association with the spinel→garnet phase transition is relaxed, a number of other potential agents for producing strain softening and localization can be considered. These include onset of dynamic recrystalization, thermal softening, metamorphic reactions, hydrothermal alteration, and hydrolytic weakening [*Kirby*, 1985; *Drury et al.*, 1991], any of which may involve changes in dominant deformation mechanism between dislocation and diffusion creep [*Karato and Wu*, 1993]. The range of possible scenarios is thereby broadened considerably and additional information is required if these possibilities are to be constrained.

Additional constraints are available from seismic reflection profiling and xenoliths from kimberlite pipes in the Slave province. As part of the LITHOPROBE Slave-Northern Cordillera Lithospheric Evolution (SNORCLE) transect a 725 km long reflection traverse was undertaken across the Proterozoic terranes of the Wopmay orogen and the western Slave province, terminating just east of Yellowknife [*Cook et al.*, 1997] (see also Figures 7 and 8). Numerous discontinuous mantle reflections are visible beneath the profile, although most do not correlate over large distances. However, a 10-12 km thick zone can be traced from the lower crust of the Fort Simpson terrane to 90-100 km beneath the Great Bear magmatic arc and Hottah terrane flattening out over a distance of 100 km before dipping eastward again toward the Slave province. The interpretation of this feature as related to Proterozoic subduction which terminated with the docking of the Fort Simpson terrane near 1845 Ma [*Villeneuve et al.*, 1991] is consistent with geological interpretation of the aeromagnetic anomalies and reflector depth ($\sim$ 100 km) below the Great Bear magmatic arc. Another band of reflections which varies in depth between 70 and 83 km begins at the western margin of the Slave province and can be followed laterally over a distance of $\sim$ 100 km. It is probably correlative with another set of reflections at the eastern end of the transect, implying that this feature underlies the entire western Slave. The observation of this second set of reflections corroborates the interpretation of H made in the previous section, and delivers additional constraints: the upper boundary of H, here associated with the Slave reflector, is sharp to seismic wavelengths implying a boundary transition no broader than 100 m; and H is likely laterally continuous over scales of 200 km or more, with little ($<$ 10 km) variation in depth over most of this range.

Xenoliths erupted from kimberlites on the Slave provide a second important source of information. The Drybones bay kimberlite [*Kretschmar*, 1997] is located some 50 km SE of Yellowknife (see Figure 7) within the sampling range represented in Plate 3. The occurrence of macrodiamonds implies that some portion of the cratonic mantle below the southwestern Slave lay within the diamond stability field at the time of kimberlite eruptions (270 Ma, 440 Ma [*Heaman et al.*, 1997]). Unfortunately, xenoliths from the Drybones pipe are strongly altered and of limited use in characterizing the underlying mantle (D. Canil, personal communication, 1997). This is not the case, however, for xenoliths from the Jericho pipe 300 km to the NE of YKA. Analysis by *Kopylova et al.* [1998] reveals a startling variety of lithologies (coarse and prophyroclastic peridotites, ecologites, megacrystalline pyroxenites, ilmenite-garnet wehrlites, and clinopyroxenites) including up to 30% eclogite, although

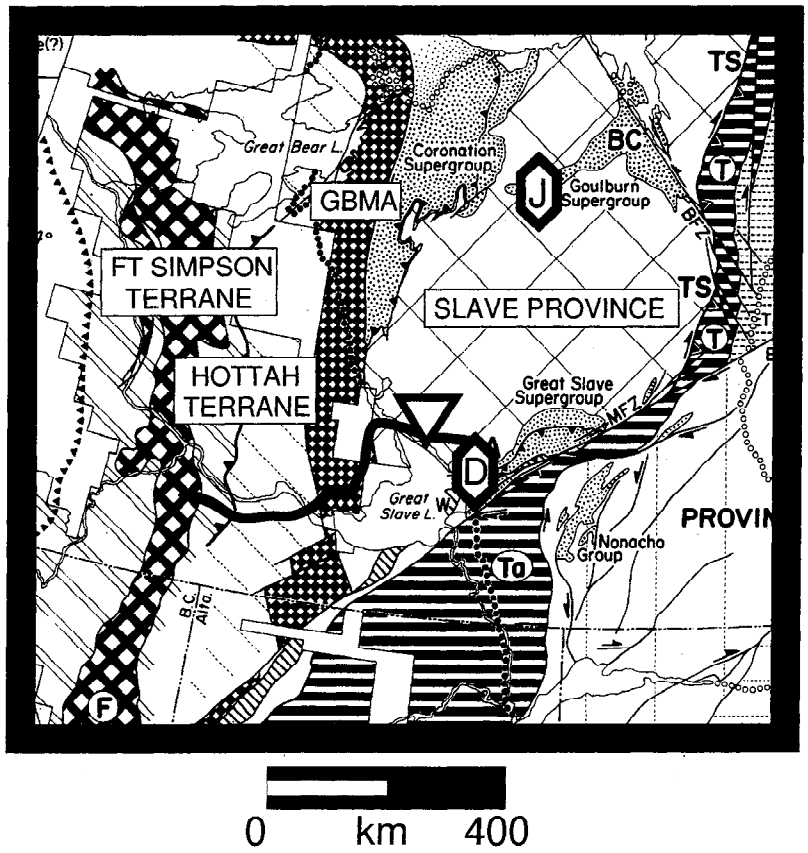

Figure 7. Geologic map from *Hoffman* [1989] showing locations of major elements of Wopmay orogen (GBMA, Great Bear magmatic arc), LITHOPROBE reflection profile (dark line), YKA (inverted triangle), and Jericho (J) and Drybones bay (D) kimberlite pipes. Used with permission from the Geological Society of America.

this likely represents an overestimate of true mantle proportions [*Schulze*, 1989]. These authors establish a petrologic stratigraphy using thermobarometry of peridotites and assign depths to orthopyroxene-free rocks on the basis of their equilibration temperatures. Porphyroclastic peridotites, wehrlites, pyroxenites, and clinopyroxenites are mapped primarily below 180 km. Eclogites have a broader distribution, and though concentrated below 120 km are also represented in the shallower (< 120 km) mantle. Eclogite is, curiously, the only lithology to show visible strain and fabric (shape preferred orientation) in thin section, whereas peridotite above 180 km is coarse and dominated by equilibrium metamorphic textures (although these may be due to recrystallization) in the Jericho pipe eclogites. It is notable that observations of eclogites from continental collision zones [*Austrheim*, 1991] suggest that, at least in some circumstances, eclogites can behave as weak, ductile materials.

The observation of strained eclogite in thin section and highly strained layers or layer sequences (H and X) within the mantle column prompts speculation into a direct association. The near horizontality, sharp contrast and lateral continuity of the layering and recognition of eclogite as the high-pressure/temperature form of oceanic basalt support a mechanism involving shallow subduction and obduction as is evidenced in the present day in central Peru and southwest Honshu [*Sacks*, 1983]. Arguments favoring widespread shallow subduction in Archean time are well established [*Vlaar*, 1986; *Helmstaedt and Schulze*, 1989; *Abbott*, 1991]. Higher temperatures inferred for the Archean [*Bickle*, 1986; *Abbott et al.*, 1994] should lead naturally to thicker oceanic crust, a more extensively depleted harzburgite mantle, and greater ridge length, all of which would be expected to result in a greater propensity for shallow subduction. Several episodes of shallow subduction would lead to a well-stratified mantle as documented here and provides the rapid cooling and thickening of lithosphere required to form diamond [*Kennedy and Kennedy*, 1976] soon after the stabilization of overlying crust [*Richardson et al.*, 1984].

In this context, H is interpreted to be a layer of slightly thicker-than-present-day (10 km) Archean oceanic crust obducted below an existing protocontinent. Appeal is once more made to transformational plasticity as a mechanism of generating large strains under relatively small applied stresses but now through the basalt → eclogite transformation [*Ruff and Kanamori*, 1983] which is accompanied by a considerably larger density increase (15%) than the spinel→garnet transformation. The development of anisotropy may thus be a transient phenomenon created within a finite depth interval and likely catalyzed by the presence of water [*Ahrens and Schubert*, 1975]. Strong (±5%) an-

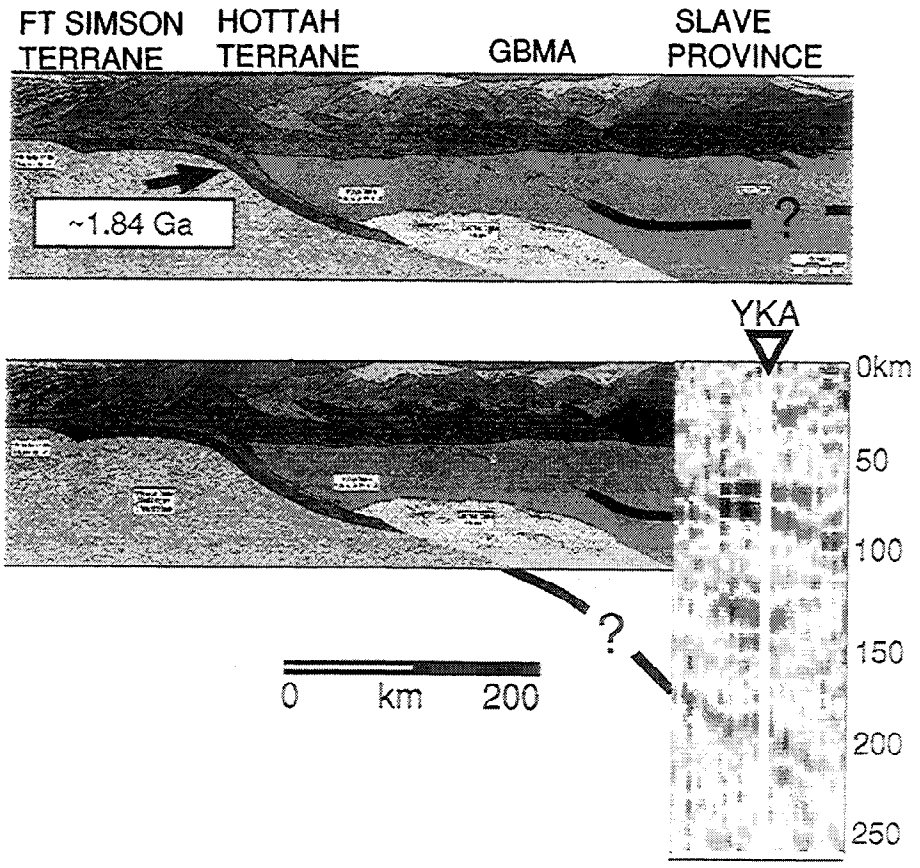

Figure 8. Integration of reflection seismic and P_{DS} profiles. (top) Interpreted reflection seismic section, courtesy of Fred Cook, with prominent mantle reflections indicated. (bottom) Juxtaposition with northern section of transverse (SH) impulse response mapped to depth. As in Figure 8, teleseismic section is distorted; however, horizontal scale at 200 km depth coincides approximately with that given by scale bar.

isotropy in eclogite is unlikely to result from lattice preferred orientation alone [*Estey and Douglas*, 1986], and it is suggested that this is supplemented by the development of a macroscopic fabric comprising compositional banding of garnet, clinopyroxene, and accessory minerals. Support for this proposal derives from analysis of eclogite xenoliths in thin section (M. Kopylova, personal communication, 1997). Abrupt localization of strain needed to account for the sharp upper boundary of H is directly enforced by the spatial extent of the former oceanic crust. The constraint of an average layer velocity comparable to that of the surroundings is accounted for by the observation that the average velocities of eclogite and peridotite closely coincide [*Leven et al.*, 1981; *Estey and Douglas*, 1986; *Gubbins et al.*, 1994]. A column of less perturbed, and depleted harzburgitic material corresponding to the mantle portion of the Archean oceanic plate extends from the bottom of H to X, where X is a second plate juxtaposed in a subsequent subduction episode. The presence of multiple layers at X complicates this interpretation but nevertheless favors a compositional layering. Development of a strong elastic anisotropy in subducted eclogite derives support from a remarkable comparison made by *Gubbins et al.* [1994]. They note that peculiar seismic phases, exhibiting velocity dispersion and apparently associated with propagation through subducted oceanic crust and mantle, are recorded in New Zealand and Japan. Moreover, the dispersion recorded at these two locations is opposite in sense, such that high-frequency precursors arrive early in New Zealand while lower-frequency energy dominates at earlier times in Japan. These apparently contradictory observations can be reconciled in the presence of a highly anisotropic eclogite layer behaving for some directions of propagation as a waveguide and for others as an antiwaveguide. Thin, high-velocity (8.6 km/s) layers between 70 and 100 km depth observed in refraction profiles beneath the Siberian craton [*Egorkin et al.*, 1987], and interpreted as due to anisotropy [*Pavlenkova et al.*, 1996], would further suggest that shallow subduction as envisaged here was widespread in the Precambrian.

Figure 8 reveals a highly suggestive geometrical association between L and the interpreted subduction thrust which merges with the Fort Simpson terrane at the western end of the reflection traverse. Dip, depth, and orientation are all broadly consistent with the interpretation that L represents a continuation of the shallower feature (or a related horizon) beneath the Slave province. Curiously, $P_L s$ is characterized by a single peak, in contrast to the layer signature that would be expected on the basis of the discussion for H above. At

this point we note only that there is some suggestion of an admittedly subtle and more intermittent layering associated with $P_L s$ in Plates 3 and 4. This subduction episode culminates the process of craton formation and, by underthrusting material emplaced in the Archean, allows for a significant depth interval between X and L wherein diamond formation could take place [*Kennedy and Kennedy*, 1976]. Models currently in favor for the formation of the Slave [e.g., *Kusky*, 1989] invoke eastward subduction of the Anton terrane and collision with an accretionary prism (Contwoyto terrane) and arc complex (Hackett River terrane). Geometrical considerations thus suggest development of H well prior to accretion and perhaps as early as 4.0 Ga, the age of the basement Acasta gneiss. We note further that the Wopmay orogen and the western margin of the Slave represent a 2-D configuration and that although H, X may be confined to the Anton terrane, L likely extends north to at least the Arctic Ocean.

There are, of course, other plausible explanations for H, X, and L, and one cannot ignore the evidence for globally distributed though laterally variable discontinuities at similar depths evident, in particular, in the long-period ScS reverberation mapping of *Revenaugh and Jordan* [1991]. It is readily conceivable that the long-period results and those shown here bear no direct association. For example, a 10 km thick, anisotropic layer embedded above and below by homogeneous material would be transparent to 200 km wavelengths (conversely, if such a layer were bounded by media of different properties it would likely behave as a discrete discontinuity; however, the most likely candidiate, the spinel→garnet transition, has already been dismissed for the present case). An alternate scenario presents H as a shear zone in generally homogenous peridotite mantle developed during rifting at some point in the history of the Slave [*Bowring and Grotzinger*, 1992]. Several objections may be raised to this proposal: (1) an overall reduction in velocities would therein be expected rather than an anisotropy which brackets the velocity of ambient mantle as is observed; (2) X must then arise through a different mechanism, since juxtaposition of multiple shear zones exhibiting different shear sense would appear implausible; (3) there is no evidence for strongly sheared peridotite from shallow mantle xenoliths at the Jericho pipe (though this could be explained through geographic separation); and (4) past and present shear zones of comparable dimension ($\sim$ 10 km thickness) exposed at the surface are usually directly associated with plate boundaries of a convergent type (e.g., GSLsz, Grenville front, San Andreas fault).

A range of alternate explanations has been proferred for L (i.e., mantle discontinuities between 150 and 250 km in depth), most of which have invoked anisotropy in some form [e.g., *Leven et al.*, 1981; *Revenaugh and Jordan*, 1991; *Karato*, 1992; *Gaherty and Jordan*, 1995]; however, compare the work by *Angel et al.* [1992]. Studies of long-period waves provide two important constraints, namely, (1) a global discontinuity at $\sim$ 200 km depth does not exist [*Shearer*, 1991], implying either intermittent occurrence or significant lateral variability, both of which are consistent with mechanical and hence anisotropic layering; and (2) mantle anisotropy appears to be restricted to levels above 200-300 km depth [*Montagner and Tanimoto*, 1991]. Again, results at shorter periods suggest the class of structures responsible for L may be more complex than a simple interface separating two media with different elastic parameters. In particular, the short-period P wave refraction data of *Leven et al.* [1981] constrain L below northern Australia to be better represented by a layer. The authors note the requirement of a sharp lower boundary and suggest a thickness of 30 km, although they acknowledge that this value is not uniquely determined by the refraction data. Structure on L as observed here and by *Revenaugh and Jordan* [1991] and *Gaherty and Jordan* [1995] who note an increase in L into Australian shield, is reminiscent of the petrologic boundary separating cold, coarse harzburgite xenoliths from hot, sheared lherzolites beneath South Africa [*Boyd and Gurney*, 1986]. This has prompted the suggestion by *Gaherty and Jordan* [1995] that L represent the base of a mechanical boundary layer within the tectosphere, perhaps reflecting the transition from slow diapiric upwelling of kimberlite magmas to more rapid ascent via fracture [*Green and Gueguen*, 1974]. This suggestion and the interpretation in terms of subduction made here for L need not be inconsistent. In a detailed investigation of eclogites from the Roberts Victor pipe, *MacGregor and Manton* [1986] note the approximate correspondence between peak eclogite concentrations at depths of 165-190 km and a number of other petrologic indicators including the inflection in geotherms commonly noted in geothermobarometric studies of South African xenoliths [*Boyd*, 1989]. These same characteristics are generally shared by xenoliths from the Jericho pipe [*Kopylova et al.*, 1998] and support the notion that subducted oceanic crust has been preferentially emplaced along or abutted against this rheological (and petrologic) boundary.

The deepest structure characterizing the upper mantle beneath YKA above the transition zone is W which marks the top of a low-velocity zone. The high frequencies constituting $P_W s$ observed here indicate that the boundary is sharp (in particular, notably sharper than the 410 km discontinuity) with perhaps some topography. A discontinuity at this depth is not in evidence in the global stacks of long-period waveforms [*Shearer*, 1991], indicating that it too must be characterized by an intermittent and/or laterally variable nature. There is, however, evidence from a growing body of studies employing different methodologies that a low-velocity zone just above (and perhaps into) the transition zone does exist locally, in the back arc region of subduction zones [*Sacks and Snoke*, 1977; *Revenaugh and Sipkin*, 1994], at continental sutures [*Nolet and Zielhuis*, 1994], and, as witnessed here, below Archean cratons [*Vinnik et al.*, 1996]. If the low-velocity zones identified in these studies have a common origin, then it is unlikely to be associated with the base of the tectosphere given the range of tectonic enviroments where it is represented. A phase transition is another unlikely explanation as this mechanism should result in an increase in density and hence velocity. Nor is a structural origin involving subducted lithosphere tenable in view of the positive Clapey-

ron slope of the olivine$\rightarrow \beta$ phase transition. The simplest explanation relies on the presence of a fluid phase, possibly emplaced through subduction processes.

Revenaugh and Sipkin [1994] postulate that W represents the upper boundary of a layer of dense silicate melt transported downward by subduction and ponded atop the 410 km discontinuity. They appeal to experimental data that suggest a density cross over between basic/ultrabasic melt and olivine-rich mantle rock at pressures above 8-10 GPa [e.g., *Stolper et al.*, 1981; *Agee and Walker*, 1993]. *Nolet and Zielhuis* [1994] elaborate in detail on potential agents (e.g., dense hydrous magnesium silicates [*Thomson*, 1992] and nominally anhydrous clinopyroxene [*Bell and Rossman*, 1992]) for water storage in subducting slabs below commonly accepted dehydration depths, and discuss their possible role in producing low-velocity zones in the transition zone. They hypothesize that water injection by subduction in Paleozoic time has led to the development of a stagnant low-velocity zone, defined by weakened shear modulus and possible creation of heavy melt, below the surface expression of the Tornquist-Tesseyre zone. A geographical context for the present case is provided by the subduction of the Farallon-Kula plate system along the northwest coast of North America in the past 100 Ma [*Engebretson and Gordon*, 1986]. The potential of such a layer as a source of metasomatic fluids and kimberlite magmas has been commented upon by *Revenaugh and Sipkin* [1994] and is consistent with the occurrence of kimberlite activity on the Slave in this time interval (72 Ma at Lac du Gras [*Heaman et al.*, 1997]), with similar correlations on the Kaapvaal craton [*Vinnik*, 1996], and with the recognition that the source of kimberlite magmas lies at great depths in or below the upper mantle [*Haggerty and Sautter*, 1990]. Nevertheless, the viability of the heavy melt explanation relies critically on an improved understanding of the role of volatiles on melt density and compressibility.

8. Concluding Remarks

The results presented here bear a number of important implications for the study of the lithospheric mantle. They indicate that high-frequency PS converted energy in the coda of P can be exploited to derive a deterministic description of mantle structure at local scales using a single broadband, three-component site, if data are well represented in epicentral distance and azimuth. Sufficient data are presently available for a number of stations in the growing global network. A major component of structural heterogeneity in the mantle below YKA appears as layered structure, which, as has been argued, is thought to reflect the importance of subduction processes in assembling the continental tectosphere. The veracity of this conclusion and its validity in a more general Precambrian context will be assessed as the results from a larger body of stations are compiled and experiments are designed to map these mantle structures over wider regions.

Acknowledgments. I am indebted to Fred Cook for furnishing the interpreted SNORCLE reflection profile, Colin Thomson for notes and algorithms on wave propagation in anisotropic media, and John Cassidy for help with figures. Thanks to David Boerner, Michael Brown, Bruce Buffett, Dante Canil, Fred Cook, Shaocheng Ji, and Maya Kopylova for helpful discussion at various stages in this work. Constructive reviews by Shun-ichiro Karato, Valerie Maupin, and Justin Revenaugh are gratefully acknowledged. The Geological Survey of Canada is thanked for providing access to the YKA data archives. This research was supported BHP Diamonds Inc., Canamera Geological Ltd., LITHOPROBE, Monopros Ltd., and the Natural Sciences and Engineering Research Council of Canada. This is LITHOPROBE publication number 929.

References

Abbott, D., The case for accretion of the tectosphere by buoyant subduction, *Geophys. Res. Lett.*, *18*, 585-588, 1991.

Abbott, D., L. Burgess, J. Longhi, and W.H.F. Smith, An empirical thermal history of the Earth's upper mantle, *J. Geophys. Res.*, *99*, 13835-13850, 1994.

Agee, C.B., and D. Walker, Olivine flotation in mantle melt, *Earth Planet. Sci. Lett.*, *114*, 315-324, 1993.

Ahrens, T.J., and G. Schubert, Gabbro-eclogite reaction rate and its geophysical significance, *Rev. Geophys.*, *13*, 383-400, 1975.

Angel, R.J., A. Chopelas, and N.L. Ross, Stability of high-density clinoenstatite at upper-mantle pressures, *Nature*, *358*, 322-324, 1992.

Austrheim, H., Eclogite formation and dynamics of crustal roots under continental collision zones, *Terra Nova*, *3*, 492-499, 1991.

Barr, K.G., Crustal refraction experiment: Yellowknife 1966, *J. Geophys. Res.*, *76*, 1929-1947, 1971.

Bell, D.R., and G.R. Rossman, Water in Earth's mantle: The role of nominally anhydrous minerals, *Science*, *255*, 1391-1397, 1992.

Bickle, M.J., Implications of melting for stabilisation of the lithosphere and heat loss in the Archaean, *Earth Planet. Sci. Lett.*, *80*, 314-324, 1986.

Bostock, M.G., A seismic image of the upper mantle beneath the North American craton, *Geophys. Res. Lett.*, *23*, 1593-1596, 1996.

Bostock, M.G., and J.F. Cassidy, Upper mantle stratigraphy beneath the southern Slave craton, *Can. J. Earth Sci.*, *34*, 577-587, 1997.

Bowring, S.A., and J. Grotzinger, Implications of new chronostratigraphy for tectonic evolution of Wopmany orogen, northwestern Canadian shield, *Am. J. Sci.*, *292*, 1-20, 1992.

Bowring, S.A., I.S. Williams, and W. Compston, 3.96 Ga gneisses from the Slave province, Northwest Territories, Canada, *Geology*, *17*, 971-975, 1989.

Boyd, F.R., High- and low-temperature garnet peridotite xenoliths and their possible relation to the lithosphere-asthenosphere boundary beneath southern Africa, in *Mantle Xenoliths*, edited by P.H. Nixon, pp. 403-412, John Wiley, New York, 1989.

Boyd, F.R., and J.J Gurney, Diamonds and the African lithosphere, *Science*, *232*, 472-476, 1986.

Cassidy, J.F., A comparison of the receiver structure beneath the stations of the Canadian National Seismograph Network, *Can. J. Earth Sci.*, *32*, 938-951, 1995.

Cook, F.A., A.J. Van der Velden, and K.W. Hall, Upper mantle reflectors beneath the SNORCLE transect: Images of the base of the lithosphere?, in *Slave-Northern Cordillera Lithospheric Evolution (SNORCLE) Transect and Cordilleran Tectonics Workshop Meeting*, edited by F. Cook and P. Erdmer, *Lithoprobe Rep. 56*, pp. 58-62, Univ. of Calgary, Calgary, Alberta, 1997.

Davis, W.J., and E. Hegner, Neodymium isotopic evidence for the tectonic assmbly of Late Archean crust in the Slave Province, northwest Canda, the use of converted phases in teleseismic body-wave forms, *Contrib. Mineral. Petrol. 111*, 493-504, 1992.

Drury, M.R., R.L.M. Vissers, D. Van der Wal, and E.H.H. Strating, Shear localisation in upper mantle peridotites, *Pure Appl. Geophys.*, *137*, 439-460, 1991.

Egorkin, A.V., S.K. Zuganov, N.A. Pavlenkova, and N.M. Chernyshev, Results of lithospheric studies from long-range profiles in Siberia, *Tectonophysics*, *140*, 29-47, 1987.

Engebretson, D.C., and R.G. Gordon, Relative motions between oceanic and continental plates in the Pacific basin, *Geol. Soc. Am., Spec. Pap. 206*, 1-59, 1986.

Estey, L.H., and B.J. Douglas, Upper mantle anisotropy: a preliminary model, *J. Geophys. Res.*, *91*, 11393-11406, 1986.

Gaherty, J.B., and T.H. Jordan, Lehmann discontinuity as the base of an anisotropic layer beneath continents, *Science 268*, 1468-1471, 1995.

Golub, G.H., M. Heath, and G. Wahba, Generalized cross-validation as a method for choosing a good ridge parameter, *Technometrics*, *21*, 215-223, 1979.

Grand, S.P., Mantle shear structure beneath the Americas and surrounding oceans, *J. Geophys. Res.*, *99*, 11591-11621, 1994.

Green, D.H., and Y. Gueguen, Origin of kimberlite pipes by diapiric upwelling in the upper mantle, *Nature*, *249* , 617-620, 1974.

Gubbins, D., A. Barnicoat, and J. Cann, Seismological constraints on the gabbro-eclogite transition in subducted oceanic crust, *Earth Planet. Sci. Lett.*, *122*, 89-101, 1994.

Gurrola, H., G.E. Baker, and J.B. Minster, Simultaneous time-domain deconvolution with application to the computation of receiver functions, *Geophys. J. Int.*, *120*, 537-543, 1995.

Haggerty, S.E., and V. Sautter, Ultradeep (greater than 300 kilometers), ultramafic upper mantle xenoliths, *Science*, *248*, 993-996, 1990.

Hales, A.L., A seismic discontinuity in the lithosphere, *Earth Planet. Sci. Lett.*, *7*, 44-46, 1969.

Harte, B., and C.J. Hawkesworth, Mantle domains and mantle xenoliths, in *Kimberlites and Related Rocks*, vol. 2, edited by J. Ross et al., *Geol. Soc. Am. Spec. Publ.*, *14*, 649-686, 1989.

Heaman, L.M., B. Kjarsgaard, R.A. Creaser, H.O. Cookenboo, and U. Kretschmar, Multiple episodes of kimberlite magamatism in the Slave province, North America, in *Slave-Northern Cordillera Lithospheric Evolution (SNORCLE) Transect and Cordilleran Tectonics Workshop Meeting*, edited by F. Cook and P. Erdmer, *Lithoprobe Rep. 56*, pp. 14-17, Univ. of Calgary, Calgary, Alberta, 1997.

Helmstaedt, H., and D.J Schulze, Southern African kimberlites and their mantle sample: Implications for Archean tectonics and lithosphere evolution, in *Kimberlites and Related Rocks*, edited by J. Ross, pp. 358-368, Blackwell, Cambridge, Mass., 1989.

Hoffman, P.F., Wopmay orogen: A Wilson cycle of early Proterozoic age in the northwest of the Canadian Shield, in *The Continental Crust and Its Mineral Deposits*, edited by D.W. Strangway, pp. 523-549, Geol. Assoc. of Can., St. John's, Nfld, 1980.

Hoffman, P.F., Continental transform tectonics: Great Slave Lake shear zone (ca. 1.9 Ga), northwest Canada, *Geology*, *15*, 785-788, 1987.

Hoffman, P.F., Precambrian geology and tectonic history of North America, in *The Geology of North America*, vol. A, edited by A.W. Bally and A.R. Palmer, pp. 447-512, Geol. Soc. of Am., Boulder, Colo., 1989.

Jordan, T.H., Composition and development of the continental tectosphere, *Nature*, *274*, 544-548, 1978.

Jordan, T.H., Structure and formation of the continental tectosphere, *J. Petrol.*, Special Lithosphere Issue, 11-37, 1988.

Karato, S., On the Lehmann discontinuity, *Geophys. Res. Lett.*, *19*, 2255-2258, 1992.

Karato, S. and P. Wu, Rheology of the upper mantle: A synthesis, *Science*, *260*, 771-778, 1993.

Kennedy, S.C., and G.C. Kennedy, The equilibrium boundary between graphite and diamond, *J. Geophys. Res.*, *81*, 2467-2470, 1976.

Kennett, B.L.N., *Seismic Wave Propagation in Stratified Media*, 342 pp., Cambridge Univ. Press, New York, 1983.

Kennett, B.L.N., The removal of free surface interactions from three-component seismograms, *Geophys. J. Int.*, *104*, 153-163, 1991.

Kind, R., G.L. Kosarev, L.K. Makeyeva, and L.P. Vinnik, Observations of laterally inhomogeneous anisotropy in the continental lithosphere, *Nature*, *318*, 358-361, 1985.

Kirby, S.H., Rock mechanics observations pertinent to the rheology of the continental lithosphere and the localization of strain along shear zones, *Tectonophysics*, *119*, 1-27, 1985.

Kopylova, M., J.K. Russell, and H. Cookenboo, Upper mantle stratigraphy of the Slave Craton, Canada: Insights into a new kimberlite province, *Geology*, *26*, 315-318, 1998.

Kretschmar, U., Drybones Bay diamondiferous kimberlite, in *1997 Prospectors and Developers Association of Canada Exploration Summary*, Prospect. and Dev. Assoc. of Can., pp. 1-10, Toronto, 1997.

Kusky, T.M.. Accretion of the Archean Slave province, *Geology*, *17*, 63-67, 1989.

Langston, C.A., Structure under Mount Rainier, Washington, inferred from teleseismic body waves, *J. Geophys. Res.*, *84*, 4749-4762, 1979.

Lehmann, I., *S* and the structure of the upper mantle, *Geophys. J. R. Astron. Soc.*, *4*, 124-137, 1961.

Leven, J.H., I. Jackson, and A.E. Ringwood, Upper mantle seismic anisotropy and lithospheric decoupling, *Nature*, *289*, 234-239, 1981.

Levin, V., and J. Park, $P - SH$ conversions in a flat-layered medium with anisotropy of arbitrary orientation, *Geophys. J. Int.*, *131*, 253-266, 1997.

MacGregor, I.D. and W.I. Manton, Roberts Victor eclogites: Ancient oceanic crust, *J. Geophys. Res.*, *91*, 14063-14079, 1986.

Mainprice, D. and P.G. Silver, Interpretation of *SKS*-waves using samples from the subcontinental lithosphere, *Phys. Earth Planet. Inter.*, *78*, 257-280, 1993.

Martin, B.E., and C.J. Thomson, Modelling surface waves in anisotropic structures, II, Examples, *Phys. Earth Planet. Inter.*, *103*, 253-279, 1998.

Montagner, J.-P., and T. Tanimoto, Global upper mantle tomography of seismic velocities and anisotropies, *J. Geophys. Res.*, *96*, 20337-20351, 1991.

Nolet, G., and A. Zielhuis, Low *S* velocities under the Tornquist-Teisseyre zone: Evidence for water injection into the transition zone by subduction, *J. Geophys. Res.*, *99*, 15813-15820, 1994.

Oldenburg, D.W., A comprehensive solution to the linear deconvolution problem, *Geophys. J. R. Astron. Soc.*, *65*, 331-337, 1981.

O'Neil, H.S.C., The transition between spinel lherzolite and garnet lherzolite and its use as a geobarometer, *Contrib. Mineral. Petrol.*, *77*, 185-194, 1981.

Owens, T.J., S.R. Taylor, and G. Zandt, Crustal structure at Regional Seismic Network stations determined from inversion of broadband teleseismic waveforms, *Bull. Seismol. Soc. Am.*, *77*, 631-662, 1987.

Pavlenkova, N.I., G.A. Pavlenkova, and L.N. Solodilov, High velocities in the upper most mantle beneath the Siberian craton, *Tectonophysics*, *262*, 51-65, 1996.

Pearson, D.G., R.W. Carlson, S.B. Shirey, F.R. Boyd, and P.H. Nixon, Stabilisation of Archaean lithspheric mantle: A Re-Os isotope study of peridotite xenoliths from the Kaapvaal craton, *Earth Planet. Sci. Lett.*, *134*, 341-357, 1995.

Petersen, N., L. Vinnik, G. Kosarev, R. Kind, S. Oreshin, and K. Stammler, Sharpness of the mantle discontinuities, *Geophys. Res. Lett.*, *20*, 859-862, 1993.

Poirier, J.P., On transformation plasticity, *J. Geophys. Res.*, *87*, 6791-6797, 1982.

Revenaugh, J., and T.H. Jordan, Mantle layering from *ScS* reverberations, 3, The upper mantle, *J. Geophys. Res.*, *96* 19781-19810, 1991.

Revenaugh, J., and S.A. Sipkin, Seismic evidence for silicate melt atop the 410-km mantle discontinuity, *Nature*, *369*, 474-476, 1994.

Richardson, S.H., J.J. Gurney, A.J. Erlank, and J.W. Harris, Origin of diamonds in old enriched mantle, *Nature, 310*, 198-202, 1984.

Ruff, L., and H. Kanamori, Seismic coupling and uncoupling at subduction zones, *Tectonophysics, 99*, 99-117, 1983.

Sacks, I.S., The subduction of young lithosphere, *J. Geophys. Res., 88*, 3355-3366, 1983.

Sacks, I.S., and J.A. Snoke, The use of converted phases to infer the depth of the lithosphere-asthenosphere boundary beneath South America, *J. Geophys. Res., 82*, 2011-2017, 1977.

Sammis, C.G. and J.L. Dein, On the possibility of transformational superplasticity in the Earth's mantle, *J. Geophys. Res., 79*, 2961-2965, 1974.

Schulze, D.J., Constraints on the abundance of eclogites in the upper mantle, *J. Geophys. Res., 94*, 4205-4212, 1989.

Shearer, P.M., Constraints on upper mantle discontinuities from observations of long-period reflected and converted phases, *J. Geophys. Res., 96*, 18147-18182, 1991.

Stammler, K., R. Kind, N. Petersen, G. Kosarev, L.P. Vinnik, and Q. Liu, The upper mantle discontinuities: Correlated or anticorrelated?, *Geophys. Res. Lett., , 15*, 1563-1566, 1992.

Stolper, E.M., D. Walker, B.H. Hager, and J.F. Hays, Melt segregation from partially molten source region, *J. Geophys. Res., 86*, 6161-6271, 1981.

Thomson, A.B., Fluids deep in the Earth's mantle, *Nature, 358*, 295-302, 1992.

Thorpe, R.I., G.L. Cumming, and J.K. Mortensen, A significant Pb isotope boundary in the Slave province and its probable relation to ancient basement in the western Slave province, in *Project summaries: Canada-Northwest Territories Mineral Development Subsidiary Agreement, Geol. Surv. Can. Open File Rep., 2484*, 179-184, 1992.

Villeneuve, M.E., R.J. Theriault, and G.M. Ross, U-Pb ages and Sm-Nd signature of two subsurface granites from the Fort Simpson magnetic high, northwest Canada, *Can. J. Earth Sci., 28*, 1003-1008, 1991.

Vinnik, L.P., Detection of waves converted from *P* to *SV* in the mantle, *Phys. Earth Planet. Inter., 15*, 39-45, 1977.

Vinnik, L.P., R.W.E. Green, J. Nicolaysen, G.L. Kosarev, and N.V. Petersen, Deep seismic structure of the Kaapvaal craton, *Tectonophysics, 262*, 67-75, 1996.

Vlaar, N.J., Archean global dynamics, *Geol. Mijnbouw., 89*, 159-164, 1986.

Webb, S.A.C., and B.J. Wood, Spinel-pyroxene-garnet relationships and their dependence on Cr/Al ratio, *Contrib. Mineral. Petrol., 92*, 471-480, 1986.

Zandt, G., and G.E. Randall, Observations of shear-coupled *P*-waves, *Geophys. Res. Lett., 12*, 565-568, 1985.

M. G. Bostock, Department of Earth and Ocean Sciences, University of British Columbia, Vancouver, British Columbia, Canada V6T 1Z4. (e-mail: bostock@geop.ubc.ca)

(Received December 1, 1997; revised March 10, 1998;
accepted March 23, 1998.)